Graphical Abstract

To create your abstract, type over the instructions in the template box below.
Fonts or abstract dimensions should not be changed or altered.

Drastic solid-state fluorescence enhancement behaviour of imidazo[4,5-*a*]naphthalene-type fluorescent hosts upon inclusion of polyethers and *t*-butyl alcohol

Leave this area blank for abstract info.

Yousuke Ooyama*, Shinobu Nagano and Katsuhira Yoshida*
Department of Material Science, Faculty of Science,
Kochi University, Akebono-cho, Kochi, 780-8520, Japan.
Fax: (+81) 88-844-8359;
E-mail: yooyama@hiroshima-u.ac.jp;
kyoshida@cc.kochi-u.ac.jp

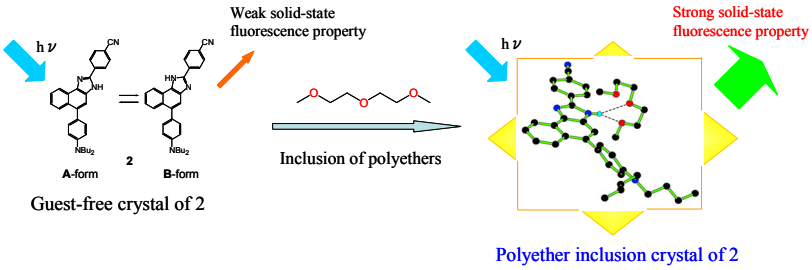

Pergamon

TETRAHEDRON

Drastic solid-state fluorescence enhancement behaviour of imidazo[4,5-*a*]naphthalene-type fluorescent hosts upon inclusion of polyethers and *t*-butyl alcohol

Yousuke Ooyama*, Shinobu Nagano and Katsuhira Yoshida*

Department of Material Science, Faculty of Science, Kochi University, Akebono-cho, Kochi 780-8520, Japan

Abstract— As one of the most promising materials for the construction of desirable solid-state fluorescent system, new solid-state fluorescent host-guest system which consists of the imidazo[4,5-*a*]naphthalene-type fluorescent hosts **2** and sterically hindered guest molecules were designed and prepared. The crystals of **2** exhibit sensitive colour change and drastic fluorescence enhancement behaviour upon polyethers (diethylene glycol dimethyl ether (DGDM), diethylene glycol diethyl ether (DGDE), and diethylene glycol dibutyl ether (DGDB)) or *t*-butyl alcohol. A comparison of the X-ray crystal structures of the guest-free and polyether- and *t*-butyl alcohol inclusion compounds indicates that the enclathrated polyether or *t*-butyl alcohol molecule decrease the π-stacking between hosts and enlarge the distance between the host–host aromatic planes. On the bases of the spectral data and the crystal structures, the effects of the enclathrated sterically hindered guest on the drastic solid-state fluorescence enhancement behaviour of the host-guest crystals are discussed.

1. Introduction

Solid-state organic fluorescent dyes have created considerable interest in recent years for their potential application to optoelectronics such as organic light emitting diode[1] and photoelectric conversion systems.[2] From the standpoint of developing an effective optoelectronics devices, many researches have been conducted on the correlation between the solid-state fluorescence properties and the molecular packing structures on the basis of the X-ray crystal structures. It has been revealed that strong intermolecular π-π interaction[3,4] or continuous intermolecular hydrogen bonding[5] between neighbouring fluorophores is a principal factor of fluorescence quenching in the solid state. Thus, the key point in design of strong solid-state fluorescent dyes is to remove the intermolecular interactions between fluorophores causing fluorescence quenching in molecular aggregation states. In particular, the introduction of bulky substituents to the original fluorophores is known to be very useful methods for solving the problem of fluorescence quenching by aggregation.[6]

On the other hand, organic fluorescent host which can exhibit sensitive colour and fluorescence changes upon formation of host-guest inclusion complexes in the crystalline state can be one of the most promising materials for the construction of desirable solid-state fluorescent system.[4,7] In the previous paper,[8] we have reported novel imidazo[4,5-*a*]naphthalene-type fluorescent clathrate host, 2-(4-cyanophenyl)-5-[4-(dibutylamino)phenyl]-3*H*-imidazo[4,5-*a*]naphthalene (**2a**) exhibiting tautomerism (**A** and **B**) on the imidazole ring. It was found that the fluorophore **2a** can include various guest molecules such as morpholine, ethanol, 1,4-dioxane, and ethyl acetate in the crystalline state by changing the toutomeric form **A** and **B**. A fluorescence enhancement and a blue-shift of the absorption and fluorescence wavelength maxima are observed depending on the enclathrated guest molecules. From the comparison of the X-ray crystal structures of the guest-free and several clathrate compounds, we have concluded the destructions of the π-π interactions between fluorophores by the enclathrated guest molecules are the main reason for the guest-dependent fluorescence enhancement and the blue-shift of the absorption and fluorescence maxima of the crystals.

Keywords: Dyes, Clathrate, Polyethers, Crystal structures, Solid-state fluorescence

* Corresponding authors. Tel.: +81 88 844 8296; fax: +81 88 844 8359.

E-mail addresses: kyoshida@cc.kochi-u.ac.jp (K. Yoshida) yooyama@hiroshima-u.ac.jp (Y. Ooyama).

In connection with this research, we have designed and prepared new solid-state fluorescent host-guest system which consists of the imidazo[4,5-*a*]naphthalene-type fluorescent host **2** and sterically hindered guest molecules such as polyethers (diethylene glycol dimethyl ether (DGDM), diethylene glycol diethyl ether (DGDE), and diethylene glycol dibutyl ether (DGDB)) and *t*-butyl alcohol. It is expected that this host-guest system with sterically hindered guest molecules causes the destructions of the π-π interactions between fluorophores comparable to the introduction of bulky substituents to the original fluorophore skeleton. Here, we report a drastic fluorescence enhancement behaviour of imidazo[4,5-*a*]naphthalene-type fluorescent hosts **2a**–**2c** upon enclathration of polyethers or *t*-butyl alcohol in the solid state. To the authors' knowledge, there is no the solid-state fluorescent host-guest system with such polethers as guest molecules. The enclathrated guest effects on the solid-state photophysical properties and the crystal packing structures of the fluorophores **2** are discussed on the basis of the results of the X-ray crystal structures of guest-inclusion compounds.

2. Results and discussion

2.1. Synthesis and spectroscopic properties of imidazo[4,5-*a*]naphthalene-type fluorescent hosts (2a–2c)

The synthetic pathway of imidazo[4,5-*a*]naphthalene-type fluorescent clathrate hosts (**2a**–**2c**) are outlined in Scheme 1. Sodium 1,2-naphthoquinone-4-sulphonate reacted with *N*, *N*-dialkylaniline in the presence of nickel(II) chloride to produce the corresponding 4-aryl-1,2-naphthoquinones **1a**–**1c** in 46–58% yield. Next, the fluorophores **2a**–**2c** were synthesized in 74–75% yield by the reaction of *p*-cyanobenzaldehyde with the corresponding **1a**–**1c**.

<Scheme 1>

The absorption and fluorescence spectra of **2a**–**2c** in benzene are shown in Figure 1. The fluorophores **2a**–**2c** exhibit intense absorption bands at 386, 386, 383 nm (ε_{max} = 27200, 27700, and 25900 $dm^3mol^{-1}cm^{-1}$, respectively) and a single intense fluorescence band at around 479, 478, and 474 nm, respectively. The fluorescence quantum yields (Φ) of **2a**–**2c** are 0.91, 0.92, and 0.89, respectively. The absorption and fluorescence maxima of **2c** are slightly blue-shifted compared to those of **2a** and **2b**, and the value Φ of **2c** is lower than those of **2a** and **2b**. This result is attributed to decrease of the π-conjugation arising from steric hindrance between 4-(diethylamino)-2-methyl-phenyl group and the imidazo[4,5-*a*]naphthalene plane of **2c**.

<Figure 1>

2.2. Preparation of guest-inclusion crystals

The preparation of polyether and *t*-butyl alcohol inclusion crystals was attempted by recrystallization from the three polyethers (DGDM, DGDE, and DGDB) and *t*-butyl alcohol solutions respectively. The hosts **2a**–**2c** formed 1 : 2 inclusion crystals with *t*-butyl alcohol. In the cases of **2a** and **2c**, the 2 : 1 inclusion crystals with DGDM, DGDE, and DGDB were obtained. On the other hand, the host **2b** formed 1 : 2 inclusion crystal with DGDM, DGDE, and DGDB. The guest-free crystal of **2a** was obtained by recrystallization of it from acetonitrile. However, in the cases of **2b** and **2c**, the guest-free crystals were not obtained, because the hosts formed inclusion crystals with either water, or guest solvent molecule, or both. We have found that the host **2a** yields inclusion compounds in stoichiometric ratios with various alcohols such as ethanol, 1-butanol, and *s*-butyl alcohol. The characteristics of polyethers and alcohols inclusion crystals of **2a**–**2c** are summarized in Table 1. Compared to the guest-free crystal of **2a**, the colour of the guest-inclusion crystals of **2a**–**2c** varied from orange to light yellow and a drastic fluorescence enhancement was observed.

<Table 1>

2.3. Solid-state fluorescence enhancement behaviour upon formation of guest-inclusion crystals

In order to investigate the effect of clathrate formation on the solid-state photophysical properties, the fluorescence excitation and emission spectra of the guest-free and the guest-inclusion crystals were measured. Compared to the guest-free crystal of **2a**, the excitation and emission maxima of the alcohol-inclusion crystals except the *s*-butyl alcohol-inclusion crystal exhibit a blue shift and the fluorescence intensity is enhanced to various degrees depending on the identity of the enclathrated alcohol molecules (Figure 2). The guest-free crystal of **2a** exhibits relatively weak fluorescence with emission maximum at 536 nm, while the alcohol-inclusion crystals exhibit much stronger fluorescence intensity with the emission maximum blue shifted to around 475–515 nm. Relative fluorescence intensity (RFI) which was determined by considering the fluorescence intensity of crystal **2a** as 1.0, increases in the following order: ethanol-inclusion crystal (RFI = 1.6) < 1-butanol-inclusion crystal (RFI = 2.6) < *t*-butyl alcohol-inclusion crystal (RFI = 4.7). The *t*-butyl alcohol-inclusion crystals exhibit the strongest fluorescence intensity of the alcohol-inclusion crystals. The fluorescence intensities of *t*-butyl alcohol-inclusion crystals of **2b** (RFI = 3.0) and **2c** (RFI = 5.8) are also stronger than those of the guest-free and alcohol-inclusion crystals of **2a**.

<Figure 2>

Of particular interest are the solid-state phtophysical properties of polyether-inclusion crystals (Figure 3). In the cases of **2a** and **2c**, the RFI is in the following order: DGDM-inclusion crystal (RFI = 2.2 for **2a** and 3.1 for **2c**) < DGDB-inclusion crystal (RFI = 3.2 for **2a** and 3.7 for **2c**) < DGDE-inclusion crystal (RFI = 6.3 for **2a** and 7.3 for **2c**). On the other hand, in the case of **2b**, the DGDM-inclusion crystal (RFI = 6.0) exhibits the strongest fluorescence intensity among the polyether-inclusion crystals (RFI = 4.1 for DGDE-inclusion crystal and 5.0 for DGDB-inclusion crystal). The fluorescence maximum of polyether-inclusion crystals shifts to shorter wavelength with an increase in the fluorescence intensity, as with the case of *t*-butyl alcohol-inclusion crystals. It is noteworthy that the emission maxima of *t*-butyl alcohol-inclusion crystals both of **2a** and **2c**, DGDE-inclusion crystal of **2b**, and DGDB-inclusion crystal of **2c** are similar to those in benzene. Consequently, these results demonstrated that the solid-state photophysical properties of the four polyether-inclusion crystals are close to their photophysical properties in solution.

<Figure 3>

2.4. Relation between the solid-state fluorescence properties and X-ray crystal structures of guest-inclusion compounds

As shown in the previous sections, the guest-free crystals of **2a** exhibit relatively weak fluorescence, whereas the polyether- and *t*-butyl alcohol-inclusion crystals of **2a**–**2c** exhibit stronger fluorescence with a blue-shifted emission maximum. The crystal structures of the guest-free crystal of **2a** and the ethanol, morpholine, 1,4-dioxane, and ethyl acetate-inclusion compounds have already been determined by X-ray diffraction and are reported in the preceding paper.[8] The packing structure of **2a** demonstrates that the crystal is built up by the π-stacking arrangements between the naphthoimidazole and the *p*-cyanophenyl moieties in the two hosts (Figure 4). We have proposed that the close π-π overlap of the host molecules causes π-π interactions, leading to the strong fluorescence quenching of the guest-free crystal. From the comparison of the X-ray crystal structures of the guest-free and the guest-inclusion compounds, we have concluded the destructions of the π-π interactions between fluorophores by the enclathrated guest molecules are the main reason for the guest-dependent fluorescence enhancement and the blue-shift of the absorption and fluorescence maxima of the crystals.

<Figure 4>

Thus, in order to investigate the enclathrated guest effects on a drastic fluorescence enhancement behaviour of the polyether- and *t*-butyl-inclusion crystals, the crystal structures of the DGDM- and *t*-butyl alcohol-inclusion compounds for **2a** and **2b** have been determined by X-ray diffraction analysis. Figures 5–8 show the X-ray crystal structures of the guest-inclusion compounds. The toutomeric forms (A and B) of imidazole ring of **2** in the crystalline state were changed depending on the enclathrated guest molecules. The tautomeric form of **2** is A-form in the crystals of **2a**·DGDM and **2b**·DGDM and B-form in the crystals of the guest-free, **2a**·*t*-butyl alcohol, **2b**·*t*-butyl alcohol. In the crystal of **2a**·DGDM, there are two crystallographically independent host molecules. These results indicate that the host **2** can include various guest molecules by changing the toutomeric form on the imidazole ring.

The crystal of **2a**·*t*-butyl alcohol is made up by the π-stacking arrangements that avoid short contacts between the chromophores. There are no short π-π contacts of less than 3.60 Å between the neighbouring fluorophores, which indicates a considerable destruction of the π-π interactions (Figures 5-(c)). An one-dimensional chain of (···H···G···G···) is formed through three-type intermolecular hydrogen bonding between host and guest and between two guests; a proton of an imidazole ring in the host is directing toward the oxygen of the guest (N(1)H(2)···O(2) angle = 173(3)°, N(1)···O(2) distance = 2.800(4) Å), the hydroxyl proton of another guest is directing toward the imino nitrogen of the host (O(1)H(25)···N(2) angle = 175(3)°, O(1)···N(2) distance = 2.799(3) Å), and the hydroxyl proton of the guest is directing toward the oxygen of another guest (O(2)H(35)···O(1) angle = 169(2)°, O(2)···O(1) distance = 2.694(3) Å) (Figure 5-(b)).

<Figure 5>

On the other hand, the crystal of **2b**·*t*-butyl alcohol is built up by the hydrogen bonded cluster unit composed of two hosts and four *t*-butyl alcohol molecules. As shown in Figures 6-(a) and (b), the hydroxyl proton of the guest is directing toward the imino nitrogen of host (O(1)H(33)···N(2) angle = 175(4)°, O(1)···N(2) distance = 2.817(5) Å) and the proton of the host is directing toward the oxygen of another guest (N(1)H(1)···O(2) angle = 176(4)°, N(1)···O(2) distance = 2.853(4) Å). In addition, the two *t*-butyl alcohol molecules are bound by intermolecular hydrogen bonds: the hydroxyl proton of the guest is directing toward the oxygen of another guest (O(2)H(43)···O(1) angle = 168(5)°, O(2)···O(1) distance = 2.815(4) Å). There are 20 (= 10×2) short interatomic contacts of less than 3.6 Å between the host molecules (Figure 6-(c)). The average distance of the interatomic π-π contacts is ca. 3.52Å, respectively, which is large distance in comparison with the guest-free crystal of **2a**.

<Figure 6>

The crystal of **2a**·DGDM is also built up by the π-stacking arrangements between the naphthoimidazole and the *p*-cyanophenyl moieties in the two hosts (Figure 7). There are 15 short interatomic π-π contacts between the two hosts. The average distance of the interatomic π-π contacts is ca. 3.47Å, which suggests π-π interactions. The two-type intramolecular hydrogen bonds are observed between the host and the guest; the proton of imidazole ring in host is directing toward the central oxygen of DGDM molecule (N(2)H(1)···O(2) angle = 171(2)˚, N(2)···O(2) distance = 2.904(3) Å) and the proton of imidazole ring in another crystallographically independent host is directing toward the side oxygen of the DGDM molecule (N(6)H(25)···O(3) angle = 175(3)˚, N(6)···O(3) distance = 2.873(3) Å). Figure 8-(a) shows the molecular packing structure for the crystal of **2b**·DGDM. There are no intermolecular hydrogen bonding interactions and no short π-π contacts of less than 3.60 Å between the neighbouring fluorophores, which indicates a considerable destruction of the π-π interactions. The intramolecular hydrogen bonds are observed between the host and the guest. As shown in Figure 8-(b), the proton of the imidazole of host have two proton acceptors and become bifurcated-donor hydrogen to form the three-centred hydrogen bonding arrangements with the central and side oxygen atoms of guest (N(2)H(1)···O(2) angle = 131(2)˚, N(2)···O(2) distance = 3.004(3) Å and N(2)H(1)···O(3) angle = 156(2)˚, N(2)···O(3) distance = 3.047(3) Å).

<Figure 7>

<Figure 8>

A comparison of the above five crystal structures confirms that the strength of the π-π interactions decreases in the following order: **2a** (guest-free) > **2a**·DGDM > **2b**·*t*-butyl alcohol > **2a**·*t*-butyl alcohol > **2b**·DGDM. As seen Figures 2 and 3, the solid-state fluorescence intensity is the reverse order. These results confirm that the differences in the destruction of the host-host π-π interactions by enclathration of the guest molecules are reflected on the solid-state fluorescence intensity of the crystals. On the other hand, in our previous works[5,8], we have demonstrated that continuous intermolecular hydrogen bonding between hosts (···H···H···) or an one-dimensional chain ranging alternately host and guest (···H···G···H···) is a principal factor of fluorescence quenching in the solid state. In the crystal of **2a**·*t*-butyl alcohol, an one-dimensional chain of (···H···G···G···) is formed through the intermolecular hydrogen bonding between host and guest and between two guests. It was considered that the continuous intermolecular hydrogen bonding of (···H···G···G···) hardly contribute to quenching of the solid-state fluorescence. Therefore, the X-ray crystal structures of the polyether- and *t*-butyl alcohol-inclusion crystals demonstrated that the destructions of the π-π interactions between host molecules by the enclathrated sterically hindered guest molecules are the main reason for a drastic fluorescence enhancement of the crystals.

3. Conclusions

As one of the most promising materials for the construction of desirable solid-state fluorescent system, we have designed and prepared the solid-state fluorescent host-guest system which consists of novel imidazo[4,5-*a*]naphthalene-type fluorescent hosts **2** and sterically hindered guest molecules such as polyethers and *t*-butyl alcohol. The host-guest crystals composed of **2** and polyethers or *t*-butyl alcohol exhibit strong solid-state fluorescence intensity compared to the guest-free crystal of **2**. The X-ray crystal structures of the polyether- and *t*-butyl alcohol-inclusion crystals demonstrated that the destructions of the π-π interactions between host molecules by the enclathrated sterically hindered guest molecules are the main reason for a drastic fluorescence enhancement of the crystals. Thus, new-type solid-state fluorescence system has been constructed by the fluorescent host and sterically hindered guest molecules. Furthermore, new useful information concerning the solid-state fluorescence has been obtained: the continuous intermolecular hydrogen bonding of (···H···G···G···) hardly contribute to quenching of the solid-state fluorescence.

4. Experimental section

4.1. General procedure

Elemental analyses were measured with a Perkin Elmer 2400 II CHN analyzer. IR spectra were recorded on a JASCO FT/IR-5300 spectrophotometer for samples in KBr pellet form. Single-crystal X-ray diffraction was performed on Rigaku AFC7S diffractometer. Absorption spectra were observed with a JASCO U-best30 spectrophotometer and fluorescence spectra were measured with a JASCO FP-777 spectrophotometer. The fluorescence quantum yields (Φ) in benzene were determined using 9,10-diphenylanthracene (Φ = 0.67, λex = 357 nm)[9] in benzene as the standard. For the measurement of the solid-state fluorescence excitation and emission spectra of the crystals, Jasco FP-1060 attachment was used. ^{1}H NMR spectra were recorded on a JNM-LA-400 (400 MHz) FT NMR spectrometer with tetramethylsilane (TMS) as an internal standard.

4.2. Synthesis

4.2.1. General synthetic procedure for 4-aryl-1,2-naphthoquinones **1a**–**1c**.

A solution of sodium 1,2-naphthoquinone-4-sulphonate (38.4 mmol), *N*,*N*-dialkylaniline (57.6 mmol), and $NiCl_2 \cdot 4H_2O$ (38.4 mmol) in CH_3COOH : H_2O [4 : 1 (v/v)] (200 ml) was stirred at room temperature for 7 days. The reaction mixture was poured into water. The solution was neutralized with aq. Na_2CO_3 and extracted with CH_2Cl_2. The organic extract was washed with water and evaporated.

The residue was chromatographed on silica gel (CH_2Cl_2 as eluent) to give **1a**–**1c**.

4.2.2. 4-[4-(Diethylamino)phenyl]-[1,2]naphthoquinone (**1a**)

Yield 58 %; mp 116-118 °C; ^{1}H NMR (400 MHz, [D_6]DMSO, TMS) δ = 1.13 (t, 6H), 3.42 (m, 4H), 6.29 (s, 1H), 6.79 (d, J = 8.7 Hz, 2H), 6.39 (d, J = 8.7 Hz, 2H), 7.61 (m, 1H), 7.72 (m, 1H), 7.72 (m, 2H), 8.03 (m, 1H); IR (KBr): $\tilde{\nu}$ = 1650, 1603 cm^{-1}; MS [m/z] %: 305 (100) [M^+].

4.2.3. 4-[4-(Dibutylamino)phenyl]-[1,2]naphthoquinone (**1b**)

Yield 50 %; mp 94-97 °C; ^{1}H NMR (400 MHz, [D_6]DMSO, TMS) δ = 0.92 (t, 6H), 1.34 (m, 4H), 1.54 (m, 4H), 3.42 (m, 4H), 6.29 (s, 1H), 6.76 (d, J = 8.9 Hz, 2H), 7.37 (d, J = 8.9 Hz, 2H), 7.53 (m, 1H), 7.61 (m, 1H), 7.72 (m, 1H), 8.02 (m, 1H); IR (KBr): $\tilde{\nu}$ = 1645, 1601 cm^{-1}.

4.2.4. 4-[4-(Diethylamino)-2-methyl-phenyl]-[1,2]naphthoquinone (**1c**)

Yield 46 %; mp 143-147 °C; ^{1}H NMR (400 MHz, $CDCl_3$, TMS) δ = 1.12 (t, 6H), 2.18 (s, 3H), 3.42 (m, 4H), 6.37 (s, 1H), 6.60 (m, 2H), 7.05 (d, J = 9.3 Hz, 1H), 7.14 (d, J = 7.8 Hz, 1H), 7.47-7.56 (m, 2H), 8.17 (m, 1H); IR (KBr): $\tilde{\nu}$ = 1654, 1608 cm^{-1}.

4.2.5. General synthetic procedure for compounds (**2a**–**2c**) by the reaction of 4-aryl-1,2-naphthoquinones (**1a**–**1c**) with *p*-cyanobenzaldehyde

A solution of **1** (18.45 mmol), *p*-cyanobenzaldehyde (18.5 mmol), and ammonium acetate (0.3 mol) in acetic acid (170 ml) was stirred at 80 ˚C for 1 h. The reaction mixture was neutralized with aq. Na_2CO_3 and extracted with CH_2Cl_2. The organic extract was washed with water and evaporated. The residue was chromatographed on silica gel (CH_2Cl_2 : ethyl acetate = 10 : 1 as eluent) to give **2**.

4.2.6. 2-(4-Cyanophenyl)-5-[4-(diethylamino)phenyl]-3*H*-imidazo[4,5-*a*]naphthalene (**2a**)

Yield 75 %; mp 244-247 °C; ^{1}H NMR (400 MHz, [D_6]SMSO, TMS) δ = 1.15 (t, 6H), 3.34 (m, 4H), 6.80 (d, J = 8.5 Hz, 2H), 7.31 (d, J = 8.3 Hz, 2H), 7.46 (m, 1H), 7.54 (s, 1H), 7.65 (m, 1H), 7.96 (d, J = 8.3 Hz, 1H), 8.04 (d, J = 8.1 Hz, 2H), 8.41 (d, J = 7.8 Hz, 2H), 8.58 (d, J = 6.6 Hz, 1H); IR (KBr): $\tilde{\nu}$ = 2220 cm^{-1}; elemental analysis calcd (%) for $C_{28}H_{24}N_4$: C 80.74, H 5.81, N 13.45; found: C 80.88, H 5.61, N 13.68.

4.2.7. 2-(4-Cyanophenyl)-5-[4-(dibutylamino)phenyl]-3*H*-imidazo[4,5-*a*]naphthalene (**2b**)

Yield 74 %; mp 198-200 °C; ^{1}H NMR (400 MHz, [D_6]SMSO, TMS) δ = 0.95 (t, 6H), 1.36 (m, 4H), 1.57 (m, 4H), 3.34 (m, 4H), 6.75 (d, J = 7.6 Hz, 2H), 7.30 (d, J = 7.3 Hz, 2H), 7.46 (m, 1H), 7.54 (s, 1H), 7.65 (m, 1H), 7.96 (d, J = 8.3 Hz, 1H), 8.04 (d, J = 6.7 Hz, 2H), 8.41 (d, J = 6.7 Hz, 2H), 8.58 (d, J = 8.3 Hz, 1H); IR (KBr): $\tilde{\nu}$ = 2217 cm^{-1}; elemental analysis calcd (%) for $C_{32}H_{32}N_4$: C 81.32, H 6.82, N 11.85; found: C 80.93, H 6.89, N 11.84.

4.2.8. 2-(4-Cyanophenyl)-5-[4-(diethylamino)-2-methyl-phenyl]-3*H*-imidazo[4,5-*a*]naphthalene (**2c**)

Yield 75 %; mp 245-248 °C; ^{1}H NMR (400 MHz, [D_6]SMSO, TMS) δ = 1.15 (t, 6H), 3.34 (m, 4H), 1.94 (s, 1H), 6.61 (m, 1H), 6.65 (s, 1H), 7.02 (d, J = 8.3 Hz, 1H), 7.41 (m, 1H), 7.47 (m, 2H), 8.04 (d, J = 8.3 Hz, 2H), 8.41 (d, J = 8.3 Hz, 2H), 8.57 (d, J = 8.1 Hz, 1H); IR (KBr): $\tilde{\nu}$ = 2225 cm^{-1}; elemental analysis calcd (%) for $C_{29}H_{26}N_4$: C 80.09, H 6.09, N 13.01; found: C 80.83, H 6.02, N 13.06.

4.3. Preparation of guest-inclusion crystals

The host compound **2** was dissolved with heating in respective guest-solvent. The solution was filtered and kept for a few days at room temperature. The crystals that formed were collected by filtration. The host (H) : guest (G) stoichiometric ratio of the inclusion compounds was determined by means of ^{1}H NMR integration and CHN analysis.

4.3.1. **2a**·ethanol (H : G = 1 : 1)

The host **2a** (420 mg) was dissolved by warming in ethanol (18 ml), and the resulting solution was allowed to stand at room temperature. The crystals (yellow, leaflet, 322 mg) were collected and dried on the filter paper. Elemental analysis calcd (%) for $C_{30}H_{30}N_4O$: C 77.89, H 6.54, N 12.11; found: C 77.60, H 6.24, N 11.92.

4.3.2. **2a**·1-butanol (H : G = 1 : 2)

The host **2a** (300 mg) was dissolved by warming in 1-butanol (5 ml), and the resulting solution was allowed to stand at room temperature. The crystals (yellow, prism, 252 mg) were collected and dried on the filter paper. Elemental analysis calcd (%) for $C_{36}H_{44}N_4O_2$: C 76.56, H 7.85, N 9.92; found: C 76.36, H 7.70, N 10.18.

4.3.3. **2a**·*s*-butyl alcohol (H : G = 1 : 1)

The host **2a** (100 mg) was dissolved by warming in *s*-butyl alcohol (28 ml), and the resulting solution was allowed to stand at room temperature. The crystals (yellow, needle, 68 mg) were collected and dried on the filter paper. Elemental analysis calcd (%) for $C_{32}H_{34}N_4O$: C 78.43, H 6.98, N 11.40; found: C 78.18, H 7.12, N 11.40.

4.3.4. **2a**·*t*-butyl alcohol (H : G = 1 : 2)

The host **2a** (100 mg) was dissolved by warming in *t*-butyl alcohol (14 ml), and the resulting solution was allowed to stand at room temperature. The crystals (yellow, prism, 99 mg) were collected and dried on the filter paper. Elemental analysis calcd (%) for $C_{36}H_{44}N_4O_2$: C 76.56, H 7.85, N 9.92; found: C 76.52, H 8.13, N 9.64.

4.3.5. **2a**·diethylene glycol dimethyl ether (H : G = 2 : 1)

The host **2a** (300 mg) was dissolved by warming in diethylene glycol dimethyl ether (2.5 ml), and the resulting solution was allowed to stand at room temperature. The crystals (yellow, prism, 178 mg) were collected and dried on the filter paper. Elemental analysis calcd (%) for $C_{69}H_{62}N_8O_3$: C 76.99, H 6.46, N 11.59; found: C 76.88, H 6.51, N 11.66.

4.3.6. **2a**·diethylene glycol diethyl ether (H : G = 2 : 1)
The host **2a** (330 mg) was dissolved by warming in diethylene glycol diethyl ether (2 ml), and the resulting solution was allowed to stand at room temperature. The crystals (yellow, needle, 225 mg) were collected and dried on the filter paper. Elemental analysis could not be performed, because the crystal was unstable at room temperature.

4.3.7. **2a**·diethylene glycol dibutyl ether (H : G = 2: 1)
The host **2a** (300 mg) was dissolved by warming in diethylene glycol dibutyl ether (6 ml), and the resulting solution was allowed to stand at room temperature. The crystals (yellow, needle, 256 mg) were collected and dried on the filter paper. Elemental analysis calcd (%) for $C_{68}H_{74}N_8O_3$: C 77.68, H 7.09, N 10.66; found: C 77.48, H 7.45, N 10.49.

4.3.8. **2b**·ethanol (H : G = 1: 1)
The host **2b** (200 mg) was dissolved by warming in ethanol (5 ml), and the resulting solution was allowed to stand at room temperature. The crystals (yellow, prism, 200 mg) were collected and dried on the filter paper. Elemental analysis calcd (%) for $C_{34}H_{38}N_4O$: C 78.73, H 7.38, N 10.08; found: C 78.46, H 7.19, N 10.82.

4.3.9. **2b**·*t*-butyl alcohol (H : G = 1 : 2)
The host **2b** (450 mg) was dissolved by warming in *t*-butyl alcohol (19 ml), and the resulting solution was allowed to stand at room temperature. The crystals (yellow, leaflet, 344 mg) were collected and dried on the filter paper. Elemental analysis calcd (%) for $C_{40}H_{52}N_4O_2$: C 77.38, H 8.44, N 9.02; found: C 77.73, H 8.74, N 9.28.

4.3.10. **2b**·diethylene glycol dimethyl ether (H : G = 1 : 1)
The host **2b** (220 mg) was dissolved by warming in diethylene glycol dimethyl ether (1 ml), and the resulting solution was allowed to stand at room temperature. The crystals (yellow, prism, 123 mg) were collected and dried on the filter paper. Elemental analysis calcd (%) for $C_{38}H_{46}N_4O_3$: C 75.22, H 7.64, N 9.23; found: C 75.19, H 7.69, N 9.23.

4.3.11. **2b**·diethylene glycol diethyl ether (H : G = 1 : 1)
The host **2b** (300 mg) was dissolved by warming in diethylene glycol diethyl ether (1 ml), and the resulting solution was allowed to stand at room temperature. The crystals (yellow, prism, 250 mg) were collected and dried on the filter paper. Elemental analysis calcd (%) for $C_{40}H_{50}N_4O_3$: C 75.68, H 7.94, N 8.83; found: C 75.98, H 8.23, N 8.77.

4.3.12. **2b**·diethylene glycol dibutyl ether (H : G = 1 : 1)
The host **2b** (300 mg) was dissolved by warming in diethylene glycol diethyl ether (1 ml), and the resulting solution was allowed to stand at room temperature. The crystals (yellow, prism, 210 mg) were collected and dried on the filter paper. Elemental analysis could not be performed, because the crystal was unstable at room temperature.

4.3.13. **2c**·*t*-butyl alcohol (H : G = 1 : 2)
The host **2c** (520 mg) was dissolved by warming in *t*-butyl alcohol (60 ml), and the resulting solution was allowed to stand at room temperature. The crystals (yellow, leaflet, 175 mg) were collected and dried on the filter paper. Elemental analysis calcd (%) for $C_{37}H_{46}N_4O_2$: C 76.78, H 8.01, N 9.68; found: C 76.62, H 8.20, N 9.70.

4.3.14. **2c**·diethylene glycol dimethyl ether (H : G = 2 : 1)
The host **2c** (300 mg) was dissolved by warming in diethylene glycol dimethyl ether (3 ml), and the resulting solution was allowed to stand at room temperature. The crystals (yellow, leaflet, 250 mg) were collected and dried on the filter paper. Elemental analysis calcd (%) for $C_{64}H_{66}N_8O_3$: C 77.23, H 6.68, N 11.26; found: C 77.18, H 6.77, N 11.26.

4.3.15. **2c**·diethylene glycol diethyl ether (H : G = 2 : 1)
The host **2c** (300 mg) was dissolved by warming in diethylene glycol diethyl ether (4 ml), and the resulting solution was allowed to stand at room temperature. The crystals (yellow, leaflet, 180 mg) were collected and dried on the filter paper. Elemental analysis calcd (%) for $C_{66}H_{70}N_8O_3$: C 77.46, H 6.89, N 10.95; found: C 77.99, H 7.04, N 11.03.

4.3.16. **2c**·diethylene glycol dibutyl ether (H : G = 2 : 1)
The host **2c** (300 mg) was dissolved by warming in diethylene glycol diethyl ether (4 ml), and the resulting solution was allowed to stand at room temperature. The crystals (yellow, leaflet, 195 mg) were collected and dried on the filter paper. Elemental analysis could not be performed, because the crystal was unstable at room temperature.

4.4. X-ray crystallographic studies

The reflection data were collected at 23 ± 1°C on a Rigaku AFC7S four-circle diffractometer by 2θ–ω scan technique, and using graphite-monochromated $Mo_{K\alpha}$ (λ = 0.71069 Å) radiation at 50 kV and 30 mA. In all case, the data were corrected for Lorentz and polarization effects. A correction for secondary extinction was applied. The reflection intensities were monitored by three standard reflections for every 150 reflections. An empirical absorption correction based on azimuthal scans of several reflections was applied. All calculations were performed using the teXsan[10] crystallographic software package of Molecular Structure Corporation. CCDC-692724 (**2a**), CCDC-692729 (**2a**·*t*-butyl alcohol), CCDC-692730 (**2a**·diethylene glycol dimethyl ether), CCDC-692731 (**2b**·*t*-butyl alcohol), and CCDC-692732 (**2b**·diethylene glycol dimethyl ether) contain the supplementary crystallographic data (see Table 3) for this paper. These data can be obtained free of charge from The Cambridge Crystallographic Data Centre via www.ccdc.cam.au.uk/data_request/cif.

4.4.1. Crystal of **2a**·*t*-butyl alcohol
The transmission factors ranged from 0.98 to 1.00. The crystal structure was solved by direct methods using SIR

92.[11] The structures were expanded using Fourier techniques.[12] The non-hydrogen atoms were refined anisotropically. Some hydrogen atoms were refined isotropically, the rest were fixed geometrically and not refined. Crystallographic data: $C_{36}H_{44}N_4O_2$, M = 564.77, monoclinic, a = 16.590(2), b = 9.337(3), c = 22.968(3) Å, β = 105.285(9)°, U = 3432.0(10) Å^3, ρ_{calcd} = 1.260 gcm^{-3}, T = 296.2K, space group P2$_1$/n (no.14), Z = 4, μ(Mo-K$_a$) = 0.68 cm^{-1}, 6279 reflections measured, 6043 unique (R_{int} = 0.033) which were used in all calculations. The final R indices [I > 2σ(I)], R1 = 0.0625, wR(F^2) = 0.139.

4.4.2. Crystal of **2a**·diethylene glycol dimethyl ether

The transmission factors ranged from 0.94 to 1.00. The crystal structure was solved by direct methods using SIR 92.[11] The structures were expanded using Fourier techniques.[12] The non-hydrogen atoms were refined anisotropically. Some hydrogen atoms were refined isotropically, the rest were fixed geometrically and not refined. Crystallographic data: $C_{62}H_{62}N_8O_3$, M = 967.22, triclinic, a = 11.526(2), b = 27.029(2), c = 9.134(2) Å, α = 91.08(1)°, β = 111.54(2)°, γ = 84.632(9)°, U = 2634.7(8) Å^3, ρ_{calcd} = 1.219 gcm^{-3}, T = 296.2K, space group P1- (no.2), Z = 2, μ(Mo-K$_a$) = 1.53 cm^{-1}, 9690 reflections measured, 9187 unique (R_{int} = 0.025) which were used in all calculations. The final R indices [I > 2σ(I)], R1 = 0.0546, wR(F^2) = 0.1262.

4.4.3. Crystal of **2b**·t-butyl alcohol

The transmission factors ranged from 0.96 to 1.00. The crystal structure was solved by direct methods using SIR 92.[11] The structures were expanded using Fourier techniques.[12] The non-hydrogen atoms were refined anisotropically. Some hydrogen atoms were refined isotropically, the rest were fixed geometrically and not refined. Crystallographic data: $C_{40}H_{52}N_4O_2$, M = 620.88, triclinic, a = 12.260(2), b = 15.046(1), c = 10.716(1) Å, α = 96.299(9)°, β = 90.19(1)°, γ = 75.561(9)°, U = 1902.0(4) Å^3, ρ_{calcd} = 1.084 gcm^{-3}, T = 296.2K, space group P1- (no.2), Z = 2, μ(Mo-K$_a$) = 0.67 cm^{-1}, 7075 reflections measured, 6688 unique (R_{int} = 0.027) which were used in all calculations. The final R indices [I > 2σ(I)], R1 = 0.0705, wR(F^2) = 0.1486.

4.4.4. Crystal of **2b**·diethylene glycol dimethyl ether

The transmission factors ranged from 0.99 to 1.00. The crystal structure was solved by direct methods using SIR 92.[11] The structures were expanded using Fourier techniques.[12] The non-hydrogen atoms were refined anisotropically. Some hydrogen atoms were refined isotropically, the rest were fixed geometrically and not refined. Crystallographic data: $C_{38}H_{46}N_4O_3$, M = 606.81, triclinic, a = 11.146(2), b = 17.006(3), c = 9.830(2) Å, α = 95.83(2)°, β = 103.82(1)°, γ = 80.45(1)°, U = 1780.5(5) Å^3, ρ_{calcd} = 1.132 gcm^{-3}, T = 296.2K, space group P1- (no.2), Z = 2, μ(Mo-K$_a$) = 0.72 cm^{-1}, 6622 reflections measured, 6269 unique (R_{int} = 0.017) which were used in all calculations. The final R indices [I > 2σ(I)], R1 = 0.0671, wR(F^2) = 0.1599.

Acknowledgments

This work was partially supported by a Grant-in-Aid for Science and Research from the Ministry of Education, Science, Sport and Culture of Japan (Grant 18350100) and by a Special Research Grant for Green Science from Kochi University.

References

1. (a) Tang, C. W.: VansSlyke, S. A. *Appl. Phys. Lett*. **1987**, *51*, 913; (b) Tang, C. W.: VansSlyke, S. A.: Chen, C. H. *J. Appl. Phys*. **1989**, *65*, 3610; (c) Wong, K.-C.: Chien, Y. -Y.: Chen, R.-T.: Wang, C.-F.: Liu, Y.-T.: Chiang, H.-H.: Hsieh, P.-Y.: Wu, C.-C.: Chou, C. H.: Su, Y. O.: Lee, G.-H.: Peng, S.-M. *J. Am. Chem. Soc*. **2002**, *124*, 11576; (d) Tonzola, C. J.: Alam, M. M.: Kaminsky, W. K.: Jenekhe, S. A. *J. Am. Chem. Soc*. **2003**, *125*, 13548; (e) Yeh, H.-C.: Chan, L.-H.: Wu, W.-C.: Chen, C.-T. *J. Mater. Chem.* **2004**, *14*, 1293; (f) Chen, C.-T. *Chem. Mater*. **2004**, *16*, 4389; (g) Chiang, C.-L.: Wu, M.-F.: Dai, D.-C.: Wen, Y.-S.: Wang, J.-K.: Chen, C.-T. *Adv. Funct. Mater*. **2005**, *15*, 231; (h) Berner, D.: Klein, C.: Nazeeruddin, M. D.: de Angelis, F.: Castellani, M.: Bugnon, P.: Scopelliti, R.: Zuppiroli, L.: Graetzel, M. *J. Mater. Chem*. **2006**, *16*, 4468.
2. (a) Wang, Z.-S.: Li, F.-Y.: Hang, C.-H.: Wang, L.: Wei, M.: Jin, L.-P.: Li, N.-Q. *J. Phys. Chem. B* **2000**, *104*, 9676; (b) Ehret, A.: Stuhl, L.: Spitler, M. T. *J. Phys. Chem. B* **2001**, *105*, 9960; (c) Hara, K.: Sato, T.: Katoh, R.: Furube, A.: Ohga, Y.: Shinpo, A.: Suga, S.: Sayama, K.: Sugihara, H.: Arakawa, H. *J. Phys. Chem. B* **2003**, *107*, 597; (d) Thomas, K. R. J.: Kin, J. T.: Hsu, Y.-C.: Ho, K.-C. *Chem. Commun*. **2005**, 4098; (e) Hagberg, D. P.: Edvinsson, T.: Marinado, T.: Boschloo, G.: Hagfeld, A.: Sun, L. *Chem. Commun*. **2006**, 2245; (f) Li, S.-L.: Jiang, K.-J.: Shao, K.-F.: Yang, L.-M. *Chem. Commun*. **2006**, 2792.
3. (a) Yeh, H.-C.: Wu, W.-C.: Wen, Y.-S.: Dai, D.-C.: Wang, J.-K.: Chen, C.-T. *J. Org. Chem*. **2004**, *69*, 6455; (b) Horiguchi, E.: Matsumoto, S.: Funabiki, K.: Matsui, M. *Bull. Chem. Soc. Jpn*. **2005**, *78*, 1167; (c) Dreuw, A.: Plötner, J.: Lorenz, L.: Wachtveitl, J.: Djanhan, J. E.: Brüning, J.: Metz, T.: Bolte, M.: Schmidt, M. U. *Angew. Chem. Int. Ed. Engl*. **2005**, *44*, 7783.
4. a) Yoshida, K.: Miyazaki, H.: Miura, Y.: Ooyama, Y.: Watanabe, S. *Chem. Lett*. **1999**, 837; (b) Yoshida, K.: Ooyama, Y.: Tanikawa, S.: Watanabe, S. *Chem. Lett*. **2000**, 714; (c) Yoshida, K.: Ooyama, Y.: Tanikawa, S.: Watanabe, S. *J. Chem. Soc. Perkin Trans. 2* **2002**, 708; (d) Ooyama, Y.: Yoshida, K. *New J. Chem*. **2005**, *29*, 1204; (e) Ooyama, Y.: Yoshida, K. *Eur. J. Org. Chem*. **2008**, *15*, 2564.
5. (a) Yoshida, K.: Uwada, K.: Kumaoka, H.: Bu, L.: Watanabe, S. *Chem. Lett*. **2001**, 808; (a) Ooyama, Y.: Nakamura, T.: Yoshida, K. *New J. Chem*. **2005**, *29*, 447.
6. (a) Langhals, H.: Potrawa, T.: Nöth, H.: Linti, G. *Angew. Chem. Int. Ed.* **1989**, *28*, 478; (b) Langhals, H.: Ismael, R.: Yürük, O. *Tetrahedron* **2001**, *56*, 5435; (c) Yoshida, K.: Ooyama, Y.: Miyazaki, H.: Watanabe, S. *J. Chem. Soc. Perkin Trans. 2* **2002**, 700; (d) Ooyama, Y.: Okamoto, T.: Yamaguchi, T.: Suzuki, T.: Hayashi, A.: Yoshida, K. *Chem.-Eur. J.* **2006**, 7827; (e) Ooyama, Y.: Harima, Y. *Chem. Lett*. **2006**, 902; (f) Ooyama, Y.: Yoshikawa, S.: Watanabe, S.: Yoshida, K. *Org. Biomol. Chem*. **2006**, *4*, 3406; (g) Ooyama, Y.: Kagawa, Y.: Harima, Y. *Eur. J. Org. Chem*. **2007**, *22*, 3613; (h) Ooyama, Y.: Mamura, T.: Yoshida, K. *Eur. J. Org. Chem*. **2007**, *30*, 5010; (i) Ooyama, Y.: Mamura, T.: Yoshida,

K. *Tetrahedron Lett*. **2007**, *48*, 5791; (j) Ooyama, Y.: Yoshikawa, S.: Watanabe, S.: Yoshida, K. *Org. Biomol. Chem*. **2007**, *5*, 1260.

7. (a) Fei, Z.: Kocher, N.: Mohrschladt, C. J.: Ihmels, H.: Stalke, D. *Angew. Chem. Int. Ed*. **2003**, *42*, 783; (b) Scott, J. L.: Yamada, T.: Tanaka, K. *New J. Chem*. **2004**, *28*, 447; (c) Imai, Y.: Murata, K.: Kawaguchi, K.: Sato, T.: Tajima, N.: Kuroda, R.: Matsubara, Y. *Chem*. *Asian*, *J*. **2008**, *3*, 625.
8. Ooyama, Y.: Nagano, S.: Okamura, M.: Yoshida, K. *Eur*. *J*. *Org*. *Chem.* DOI: 10.1002/ejoc.200800832.
9. Heller, C. A.: Henry, R. A.: Mclaughlin, B. A.: Bills, D. E. *J. Chem. Eng. Data* **1974**, *19*, 214.
10. *teXsan*: Crystal Structure Analysis Package, Molecular Structure Corporation **1985** and **1992**.
11. Altomare, A.: Burla, M. C.: Camalli, M.: Cascarano, M.: Giacovazzo, C.: Guagliardi, A.: Polidori, G. *J. Appl. Cryst*. **1994**, *27*, 435.
12. DIRDIF94. Beurskens, P. T.: Admiraal, G.: Beurskens, G.: Bosman, W. P.: de Gelder, R.: Israel, R.: Smits, J. M. M. The DIRIF94 program system, Technical Report of the Crystallography Laboratory, University of Nijmegen, The Netherlands, **1994**.

Captions

Scheme 1. (i) **1a**: *N*,*N*-dialkylaniline, $NiCl_2 \cdot 4H_2O$, CH_3COOH : H_2O [4 : 1 (v/v)], 7 days, RT, 58% for **1b**, 50% for **1b**, and 46% for **1c**; (ii) *p*-cyanobenzaldehyde, CH_3COONH_4, CH_3COOH, 1 h, 80 ˚C, 75% for **1b**, 74% for **1b**, and 75% for **1c**.

Figure 1. Normalized absorption (···) and fluorescence (–) spectra of **2a**–**2c** in benzene.

Figure 2. Solid-state excitation (···) and fluorescence (–) spectra of the guest-free and the alcohol inclusion crystals of **2a**–**2c**; (a) **2a** (guest-free): λ_{ex} = 451 nm, λ_{em} = 536 nm; (b) **2a**·ethanol: λ_{ex} = 451 nm, λ_{em} = 515 nm; (c) **2a**·1-butanol: λ_{ex} = 446 nm, λ_{em} = 499 nm; (d) **2a**·*s*-butyl alcohol: λ_{ex} = 442 nm, λ_{em} = 494 nm; (e) **2a**·*t*-buty alcohol: λ_{ex} = 440 nm, λ_{em} = 481 nm; (f) **2b**·*t*-buty alcohol: λ_{ex} = 443 nm, λ_{em} = 492 nm; (g) **2c**·*t*-buty alcohol: λ_{ex} = 439 nm, λ_{em} = 475 nm.

Figure 3. Solid-state excitation (···) and fluorescence (–) spectra of the guest-free and the polyether inclusion crystals of **2a**–**2c**; (a) **2a** (guest-free): λ_{ex} = 451 nm, λ_{em} = 536 nm; (b) **2a**·DGDM: λ_{ex} = 444 nm, λ_{em} = 493 nm; (c) **2a**·DGDE: λ_{ex} = 444 nm, λ_{em} = 495 nm; (d) **2a**·DGDB: λ_{ex} = 444 nm, λ_{em} = 497 nm; (e) **2b**·DGDM: λ_{ex} = 446 nm, λ_{em} = 500 nm; (f) **2b**·DGDE: λ_{ex} = 430 nm, λ_{em} = 479 nm; (g) **2b**·DGDB: λ_{ex} = 447 nm, λ_{em} = 497 nm.; (h) **2c**·DGDM: λ_{ex} = 447 nm, λ_{em} = 494 nm; (i) **2c**·DGDE: λ_{ex} = 440 nm, λ_{em} = 480 nm; (j) **2c**·DGDB: λ_{ex} = 435 nm, λ_{em} = 474 nm.

Figure 4. Crystal structure of **2a** : (a) a stereoview of the molecular packing structure and (b) top view of the pairs of fluorophores.

Figure 5. Crystal structure of **2a**·*t*-butyl alcohol : (a) a stereoview of the molecular packing structure, and (b) schematic structure, and (c) top view of the pairs of fluorophores.

Figure 6. Crystal structure of **2b**·*t*-butyl alcohol : (a) a stereoview of the molecular packing structure, and (b) schematic structure, and (c) top view of the pairs of fluorophores.

Figure 7. Crystal structure of **2a**·DGDM: (a) a stereoview of the molecular packing structure, and (b) schematic structure, and (c) top view of the pairs of fluorophores.

Figure 8. Crystal structure of **2b**·DGDM: (a) a stereoview of the molecular packing structure, and (b) schematic structure, and (c) top view of the pairs of fluorophores.

Table 1 Host–guest molar ratio, crystal form, and crystal color of the guest-free and the guest-inclusion crystals of **2a**–**2c**

Table 1 Host–guest molar ratio, crystal form, and crystal color of the guest-free and the guest-inclusion crystals of **2a**–**2c**

Host	Guest	Host : Guest (molar ratio)	Crystal form	Crystal colour
	None	1 : 0	Prism	Yellowish orange
	Ethanol	1 : 1	Leaflet	Yellowish orange
	1-Butanol	1 : 2	Prism	Yellow
2a	s-Butyl alcohol	1 : 1	Needle	Yellow
	t-Butyl alcohol	1 : 2	Leaflet	Yellow
	DGDM	2 : 1	Prism	Yellow
	DGDE	2 : 1	Needle	Yellow
	DGDB	2 : 1	Needle	Yellow
2b	*t*-Butyl alcohol	1 : 2	Leaflet	Yellow
	DGDM	1 : 1	Prism	Yellow
	DGDE	1 : 1	Prism	Light yellow
	DGDB	1 : 1	Prism	Yellow
2c	*t*-Butyl alcohol	1 : 2	Leaflet	Yellow
	DGDM	2 : 1	Leaflet	Light yellow
	DGDE	2 : 1	Leaflet	Light yellow
	DGDB	2 : 1	Leaflet	Light yellow

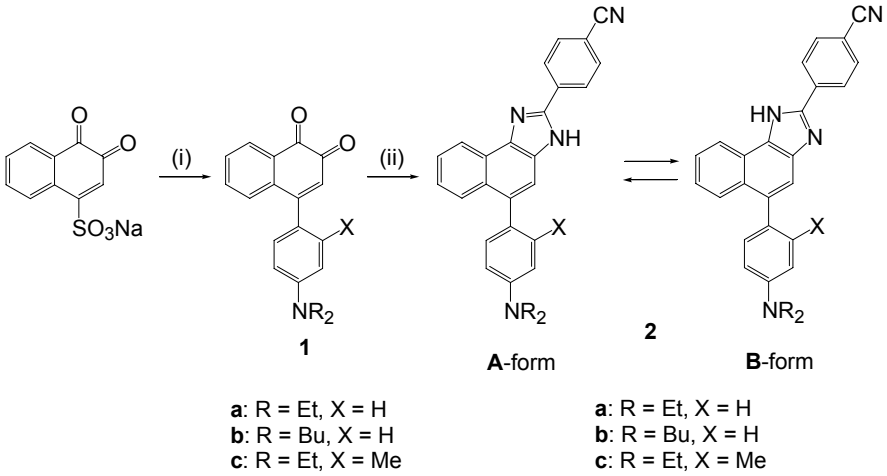

Scheme 1. (i) **1a**: *N*,*N*-dialkylaniline, $NiCl_2 \cdot 4H_2O$, CH_3COOH : H_2O [4 : 1 (v/v)], 7 days, RT, 58% for **1b**, 50% for **1b**, and 46% for **1c**; (ii) *p*-cyanobenzaldehyde, CH_3COONH_4, CH_3COOH, 1 h, 80 ˚C, 75% for **1b**, 74% for **1b**, and 75% for **1c**.

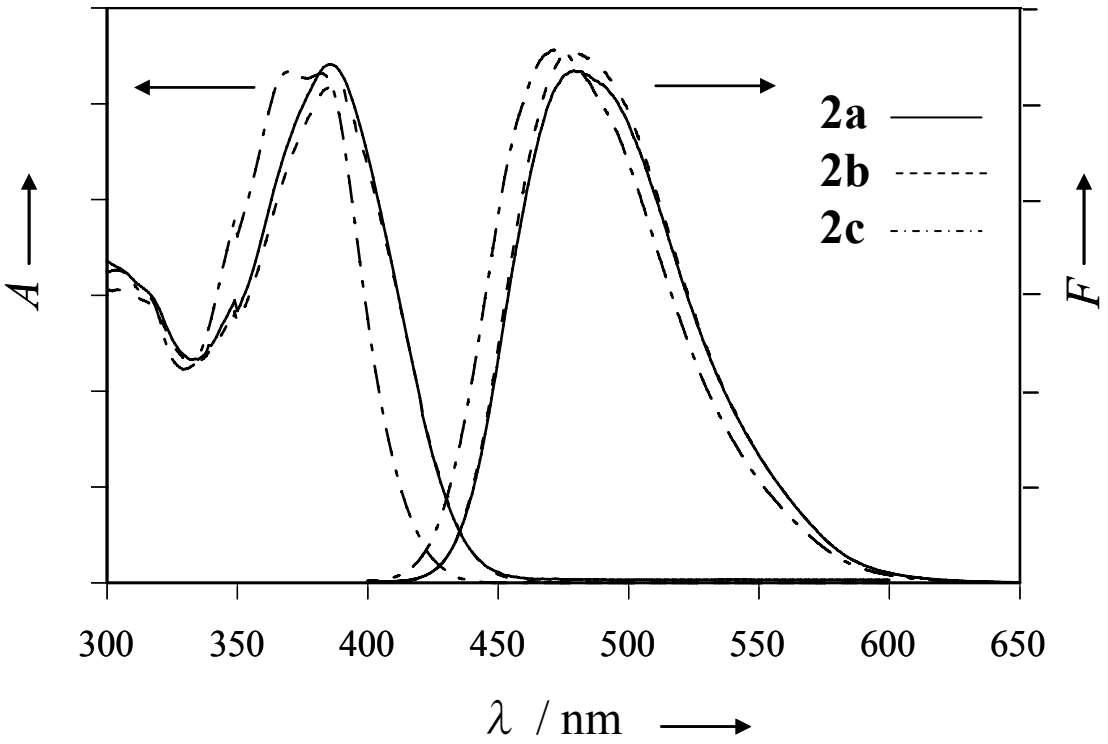

Figure 1. Normalized absorption (···) and fluorescence (–) spectra of **2a**–**2c** in benzene.

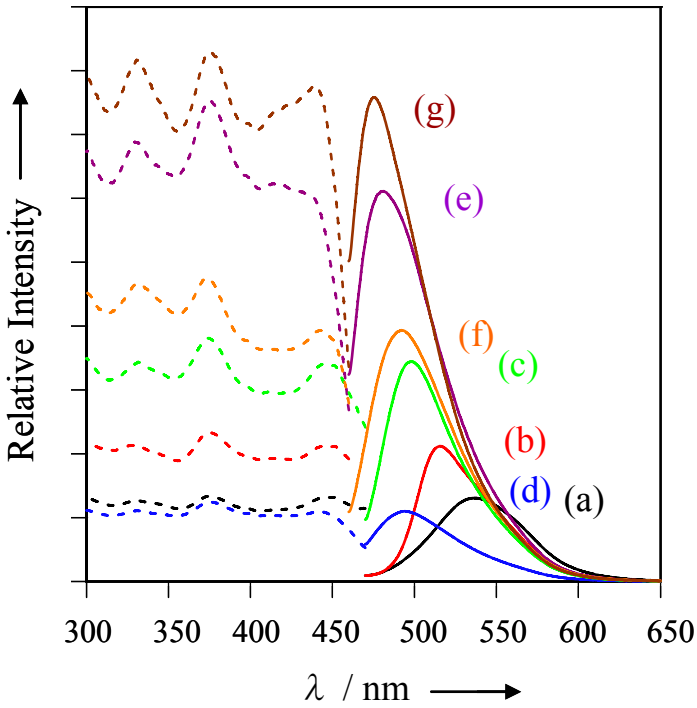

Figure 2. Solid-state excitation (···) and fluorescence (–) spectra of the guest-free and the alcohol inclusion crystals of **2a**–**2c**; (a) **2a** (guest-free): λ_{ex} = 451 nm, λ_{em} = 536 nm; (b) **2a**·ethanol: λ_{ex} = 451 nm, λ_{em} = 515 nm; (c) **2a**·1-butanol: λ_{ex} = 446 nm, λ_{em} = 499 nm; (d) **2a**·*s*-butyl alcohol: λ_{ex} = 442 nm, λ_{em} = 494 nm; (e) **2a**·*t*-buty alcohol: λ_{ex} = 440 nm, λ_{em} = 481 nm; (f) **2b**·*t*-buty alcohol: λ_{ex} = 443 nm, λ_{em} = 492 nm; (g) **2c**·*t*-buty alcohol: λ_{ex} = 439 nm, λ_{em} = 475 nm.

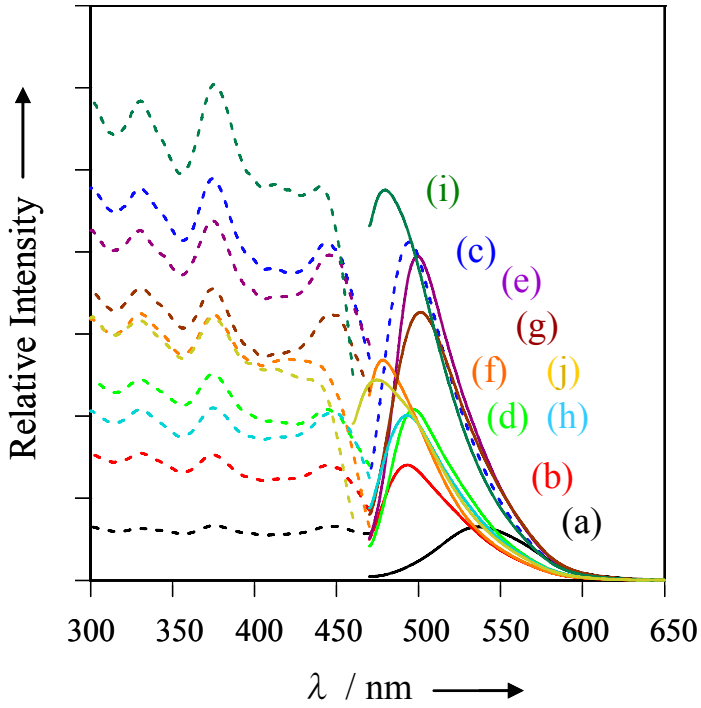

Figure 3. Solid-state excitation (···) and fluorescence (–) spectra of the guest-free and the polyether inclusion crystals of **2a**–**2c**; (a) **2a** (guest-free): λ_{ex} = 451 nm, λ_{em} = 536 nm; (b) **2a**·DGDM: λ_{ex} = 444 nm, λ_{em} = 493 nm; (c) **2a**·DGDE: λ_{ex} = 444 nm, λ_{em} = 495 nm; (d) **2a**·DGDB: λ_{ex} = 444 nm, λ_{em} = 497 nm; (e) **2b**·DGDM: λ_{ex} = 446 nm, λ_{em} = 500 nm; (f) **2b**·DGDE: λ_{ex} = 430 nm, λ_{em} = 479 nm; (g) **2b**·DGDB: λ_{ex} = 447 nm, λ_{em} = 497 nm.; (h) **2c**·DGDM: λ_{ex} = 447 nm, λ_{em} = 494 nm; (i) **2c**·DGDE: λ_{ex} = 440 nm, λ_{em} = 480 nm; (j) **2c**·DGDB: λ_{ex} = 435 nm, λ_{em} = 474 nm.

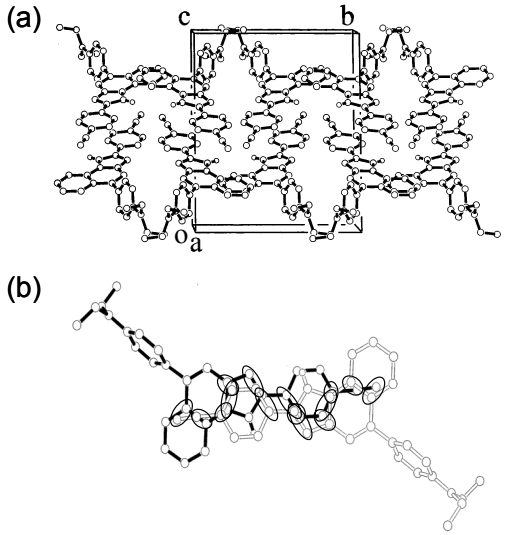

Figure 4. Crystal structure of **2a** : (a) a stereoview of the molecular packing structure and (b) top view of the pairs of fluorophores.

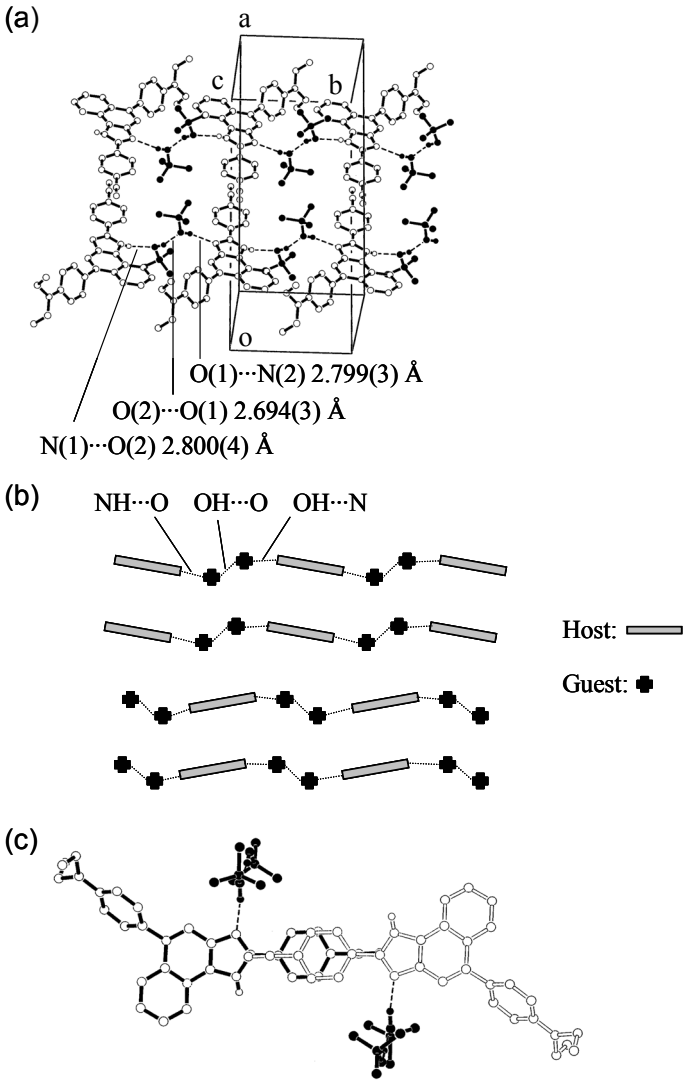

Figure 5. Crystal structure of **2a**·*t*-butyl alcohol : (a) a stereoview of the molecular packing structure, and (b) schematic structure, and (c) top view of the pairs of fluorophores.

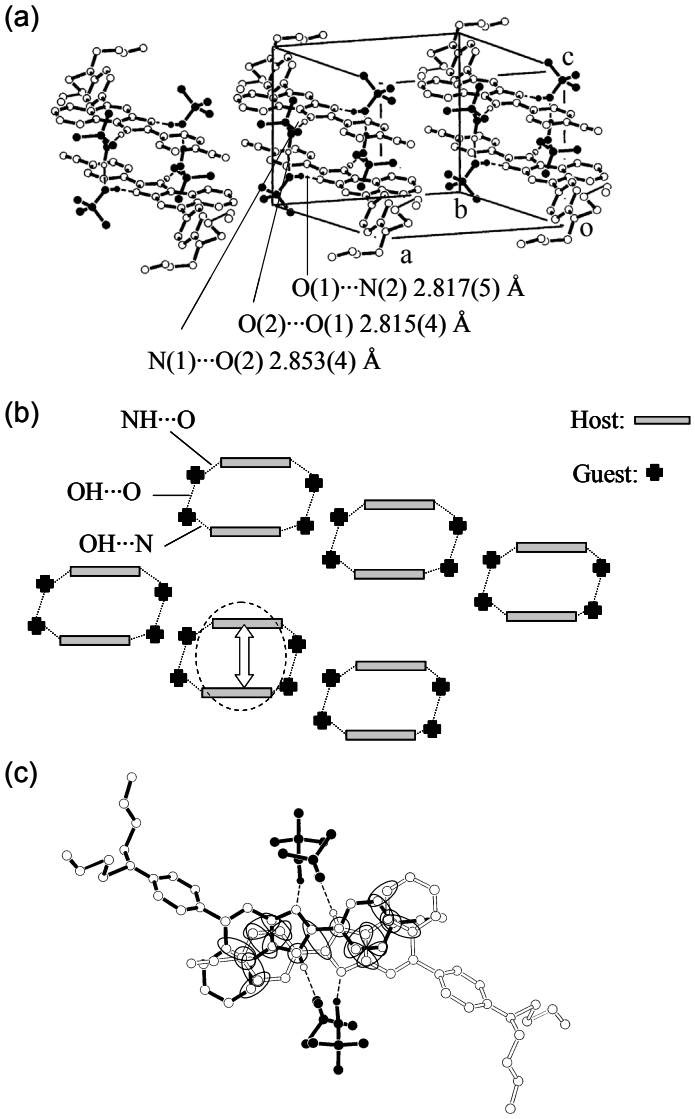

Figure 6. Crystal structure of **2b**·*t*-butyl alcohol : (a) a stereoview of the molecular packing structure, and (b) schematic structure, and (c) top view of the pairs of fluorophores.

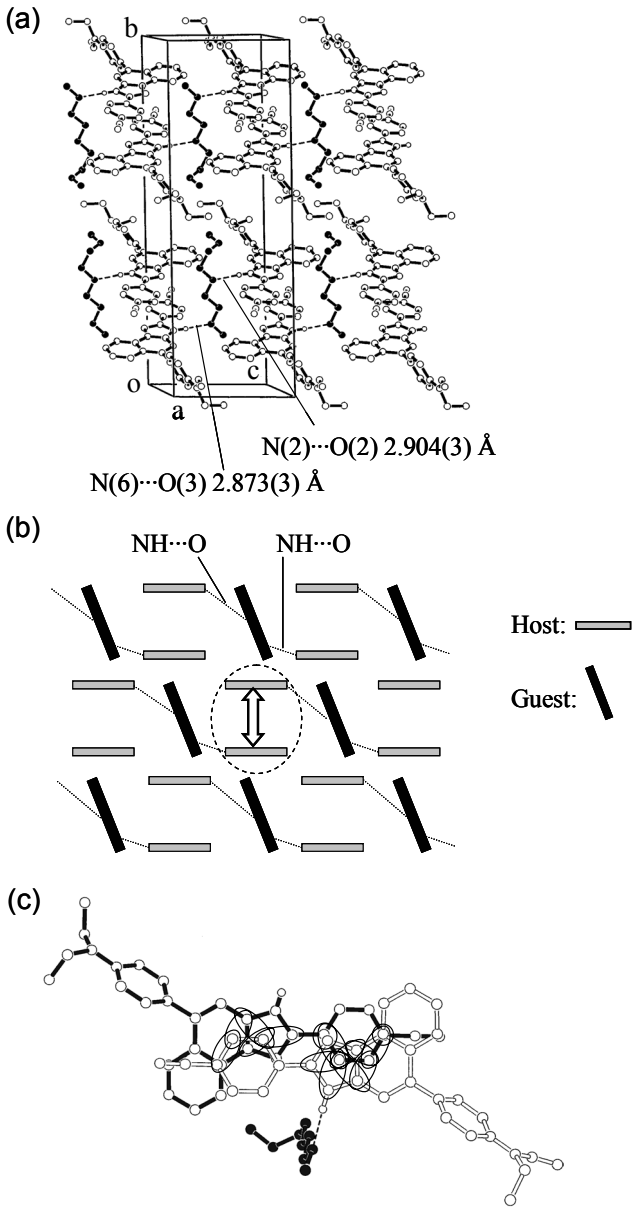

Figure 7. Crystal structure of **2a**·DGDM: (a) a stereoview of the molecular packing structure, and (b) schematic structure, and (c) top view of the pairs of fluorophores.

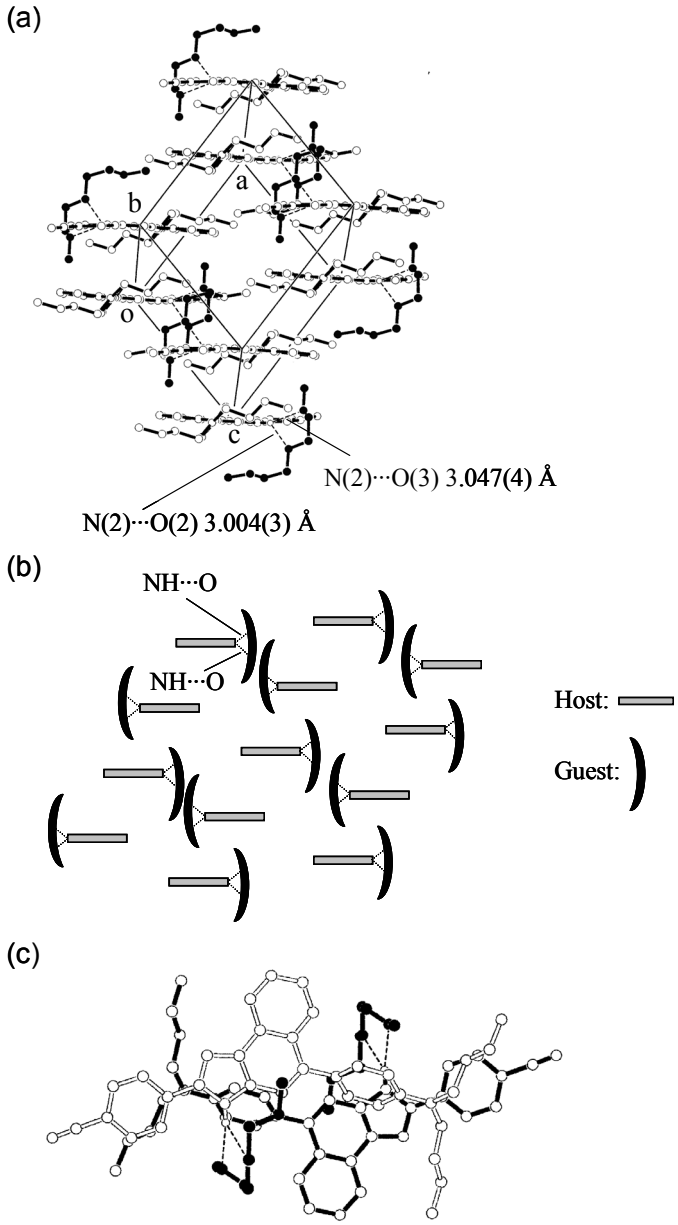

Figure 8. Crystal structure of **2b**·DGDM: (a) a stereoview of the molecular packing structure, and (b) schematic structure, and (c) top view of the pairs of fluorophores.